Journal of Fluids and Structures 118 (2023) 103844

Contents lists available at ScienceDirect

Journal of Fluids and Structures

journal homepage: www.elsevier.com/locate/jfs

An experimental investigation of the influence of inter-turbine spacing on the loads and performance of a co-planar tidal turbine fence

J. McNaughton, S. Ettema, F. Zilic de Arcos, C.R. Vogel, R.H.J. Willden *

Department of Engineering Science, University of Oxford, UK

ARTICLE INFO

Article history:
Received 18 January 2022
Received in revised form 25 January 2023
Accepted 4 February 2023
Available online 14 March 2023

Keywords:
Tidal stream energy
Tidal turbines
Constructive interference
Towing tank

ABSTRACT

Multi-rotor tidal turbine systems offer engineering benefits through shared infrastructure and improved opportunities for maintenance. Additionally, the ability to specify accurately the inter-turbine spacing in co-planar arrays allows rotors to be designed and deployed to benefit from the constructive interference effects available from neighbouring rotors. In this work we consider the effect of inter-turbine spacing and control of this spacing for a fence of turbines in low overall levels of global blockage (4.5%). We conduct experiments in a towing tank using two tidal turbine models that were previously designed to benefit from constructive interference effects at high local blockage, i.e. close inter-turbine spacing. The turbines were towed in a side-by-side configuration by suspending them from above. By making use of the tank's side wall to act as a symmetry plane we were able to emulate a fence of four laterally arrayed turbines. As indicated by theory, decreasing inter-turbine spacing is shown to have a positive effect on fence performance. By reducing the inter-turbine spacing from one diameter to a quarter of a diameter, we observe an overall 1.4% performance increase, which is driven by a 2.8% increase in the inboard turbine's power coefficient. This research is a first attempt to quantify constructive interference effects for a four turbine fence; the methods and results will be used to instruct further studies to aid the development of such multi-rotor tidal turbine systems.

1. Introduction

Over a decade's experience of deploying tidal stream turbines offshore has led to growing confidence in technology concepts, although cost reductions are still necessary so that the tidal energy industry can compete with other renewable energy technologies (ORE Catapult, 2018). Economies of scale are not yet sufficient, and innovations to produce significant cost reductions for the industry are highly desirable. One promising avenue seeks to take advantage of blockage effects. Garrett and Cummins (2007) demonstrated that the power potential of a turbine in a channel increases as a function of the blockage ratio (the ratio of turbine frontal area to channel cross-sectional area). Their theoretical model showed that to fully realise the potential improvement in turbine power requires the resistance presented by the turbine to increase with blockage ratio.

* Corresponding author.
E-mail addresses: j.mcnaughton@marin.nl (J. McNaughton), federico.zilic@univ-lehavre.fr (F. Zilic de Arcos), christopher.vogel@eng.ox.ac.uk (C.R. Vogel), richard.willden@eng.ox.ac.uk (R.H.J. Willden).

https://doi.org/10.1016/j.jfluidstructs.2023.103844

Nishino and Willden (2012) considered the problem of large cross-stream fences of turbines partially spanning the width of much wider channels, defining both a global and a local blockage ratio. Global blockage, B_G, was defined as the area ratio of all turbines to that of the channel cross-section, and local blockage, B_L, as the ratio of an individual turbine's frontal area to the cross-sectional area of the local flow passage bounded between neighbouring turbines, the sea surface and seabed. Nishino and Willden demonstrated that the maximum power of the fence increases as the local blockage is increased (i.e. by reducing inter-turbine spacing), until the turbine spacing is too close and a choking effect develops that limits the flow passing through the array, constraining and then reducing overall power. Importantly, their work demonstrated that benefits to turbine performance can be achieved for low global blockages (including as $B_G \rightarrow 0$).

The optimal arrangement with regards to performance for horizontal axis tidal turbines has been shown to be a lateral fence of co-planar rotors (Hunter et al., 2015). This has also been observed for some operational strategies of vertical axis turbines by Li and Cališal (2010). Cooke et al. (2015) used a cross-stream arrayed fence of 8 porous disks to quantify the impact of the fence-arrayed disk resistance on the flow. Using disks of different porosities and by varying inter-disk spacing, Cooke et al. demonstrated an increase in inferred performance down to a spacing of 0.2 diameters, before observing flow choking at closer spacings. It was observed that performance was not uniform across the fence. Cooke et al. proposed that end effects, i.e. reduced performance for the outer disks of the fence, were responsible for a departure in overall fence performance from theoretical models developed for very long fences of turbines. Olczak et al. (2016) compared RANS-BE (Reynolds Averaged Navier–Stokes embedded Blade Element method) simulations to experiments with small rotors of the same size and tested in the same flume as the disk experiments of Cooke et al. (2015). Olczak et al. demonstrated that increasing the global or local blockage of a co-planar rotor fence led to an increase in thrust across the fence. For a fence of five turbines they observed minor end effects; that the thrust of the outboard rotors was approximately 1% lower than for the inboard rotors. Vogel and Willden (2017) used RANS-BE to investigate inter-turbine spacing and varying turbine control for a fence of four turbines. Vogel and Willden showed how the non-uniform fence loads, associated with the outboard rotors' end effects, can be re-balanced by operating the outboard turbines at higher tip-speed ratios so that they apply greater resistance to the flow as it attempts to divert around the ends of the fence.

While the above studies focused on increasing local blockage through inter-turbine spacing, similar effects can also be achieved by positioning a turbine close to the free surface or other flow boundary. A key difference between using free-surface proximity and inter-turbine spacing to enhance local blockage effects is that the free surface can deform and hence the local blockage is difficult to measure on control precisely. Beneficial effects on interference from free-surface proximity were observed experimentally by Kolekar et al. (2019), who demonstrated an increase in power coefficient with a decrease in distance between the rotor and free surface, until a choking effect was observed, in a similar manner as discussed for the partial fence of Nishino and Willden (2012). Free surface proximity effects were also observed by Bahaj et al. (2007), who considered two tip-submersion depths. Contradictively, they observed consistently lower power and thrust coefficients for their tests with the turbine operating closer to the free surface. Additionally, blades operating near the surface may be more prone to cavitation and susceptible to fatigue from wave-induced loading.

The performance benefits experienced through local blockage may be further enhanced by designing and operating rotors for close proximity operation that maximises their mutual constructive interference. Schluntz and Willden (2015) demonstrated computationally that a rotor designed for unblocked conditions will experience a performance uplift when operated in a channel with a constrained cross-section. Maximum uplift is achieved when the turbine operates at a higher rotational speed, and thus increased thrust, compared to unblocked conditions. However, Schluntz and Willden further demonstrated that even greater performance may be achieved through the use of rotors that have been designed specifically for operation in higher blockage condition, so as to achieve an increased local thrust coefficient along the blade length that allows high thrust operation at without the requirement to increase the operating tip-speed ratio (TSR).

Large-scale experiments of multiple tidal turbines with an emphasis on performance investigation have been conducted by Noble et al. (2020) and McNaughton et al. (2022), both using the FloWave Ocean Energy Research facility. Noble et al. (2020) demonstrated a 10% increase in power and an accompanying 7% increase in thrust for a turbine placed in the accelerated bypass flow downstream of an upstream pair of turbines, although they were not able to account for the increased blockage ratio from the upstream rotors. McNaughton et al. (2022) demonstrated similar improvements in performance, with a 10.8% increase in power coefficient for a 5.2% increase in thrust for side-by-side rotors after accounting for differences in global blockage.

While array end-effects have been discussed in several studies (e.g. Cooke et al., 2015; Olczak et al., 2016; Vogel and Willden, 2017), there are limited experimental data available at a sufficiently large physical scale to ensure post-critical turbulent boundary layer flow over blades as well as at a modest global blockage ratio. In this paper we address this by considering a lateral fence of turbines with rotors designed with constructive interference principles, intending to inform design methods for turbine fences and their control. To do so, we expand the twin turbine tests of McNaughton et al. (2022) into a four-turbine fence. Tests are completed at the SSPA towing tank in Gothenburg, Sweden, with two side-by-side turbines positioned close to a tank side wall to act as symmetry plane and hence represent a pseudo four-turbine fence. Our objective is to demonstrate the effect of inter-turbine spacing on the loads at three scales: first, the overall fence performance; secondly we consider differences between inboard and outboard rotors; and finally we report blade root bending measurements as a function of azimuth position so to understand boundary and turbine interaction. Although our method allows us to draw conclusions to meet our objectives, we also discuss the arising uncertainties and potential errors associated with using the towing tank side wall as a symmetry plane. The next section describes the models, facility, and tests conducted. Section 3 presents the methodology adopted to process and present data, with discussion considering the effect of towing speed on results. Results are presented in Section 4 on the impact of inter-turbine spacing and turbine control on turbine and fence performance. We conclude with the key findings and proposed future steps of this research.

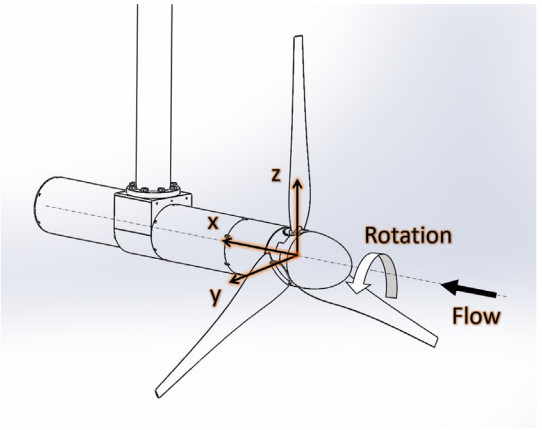

(a) Turbine schematic. As drawn, the thrust and torque are the force acting in and the moment about the x-axis respectively. For the vertical blade drawn the flapwise and edgewise Root Bending Moments (RBMs) are about the y- and x-axes respectively.

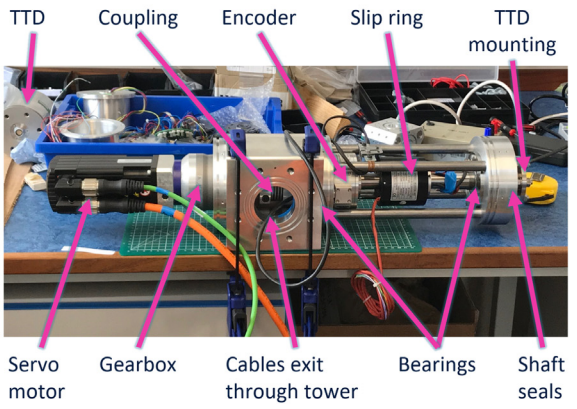

(b) Photograph of drivetrain during assembly, highlighting key components (TTD is the Thrust and Torque transducer).

Fig. 1. The experimental turbine model.

2. Experimental setup

2.1. Turbine models

Two identical 1.2 m diameter (d) turbines were used in the tests. The rotors were designed to benefit from constructive interference effects and operate in a high local blockage flow with $B_L = 37.7\%$ (see Cao et al., 2018). The rotors were previously tested at FloWave to demonstrate the performance uplift in moving from a single to twin rotor configuration at this local blockage (McNaughton et al., 2019). Those previous experiments used the University of Edinburgh's nacelles and drivetrains, originally developed for rotors of the same size (Payne et al., 2017), whereas the present tests used new ones. The approach of Payne et al. (2017) was adopted, specifically using a customised thrust and torque transducer upstream of any bearings and seals to measure rotor loads. The main difference with these new drivetrains was the use of a gearbox to reduce the difficulties found in controlling high torque at low speed described by McNaughton et al. (2019). Blade root bending moment (RBM) transducers were used to measure individual blade loads in both flapwise (out-of-plane) and edgewise (in-plane) directions. A shaft encoder upstream of the gearbox provided the rotational speed and angular position of the blades. An image of the assembled turbine and a photograph of the turbine drivetrain are provided in Fig. 1, with further details on the specific components given in Appendix A.

Although of identical design, the physical turbine models had differences within tolerance for the component manufacture and assembly. This discrepancy was assessed for tests with the turbines spaced equally between each other and the tank walls; in these tests, the average difference between the measured thrust and torque was found to be less than 1%, and that of the rotational speed about 0.1%.

2.2. Experimental setup

Tests were carried out at the 260 m long towing tank at SSPA[1] in Gothenburg, Sweden. The towing tank is 10 m wide and 5 m deep with the ability to tow at speeds up to 11 m/s, although tow speeds for the present tests were limited to 1 m/s in order to keep the predicted loads and rotational speeds within acceptable ranges for the model components and sensors. Three experimental configurations were investigated during the test campaign. In all cases the rotors were co-planar and supported from above. In the first set of tests the turbines were arranged either side of the tank centreline, in the second the turbines were arranged close to the tank side wall, and in the third a towed hydrodynamic end wall was used. For the latter two configurations, the tank side wall was used as a symmetry plane thus enabling the simulation of a four-turbine array. The symmetry plane will produce an asymmetric rotation in the turbine image system. Thus the array will be fully symmetric around the array centreline with an equal number of clockwise and anti-clockwise rotating turbines as is found in commercial arrays of tidal turbines. This paper focuses on the results from the second of these configurations, examining how inter-turbine spacing affects the performance and loads of a four-turbine fence.

[1] https://www.sspa.se/our-facilities-and-tools/towing-tank.

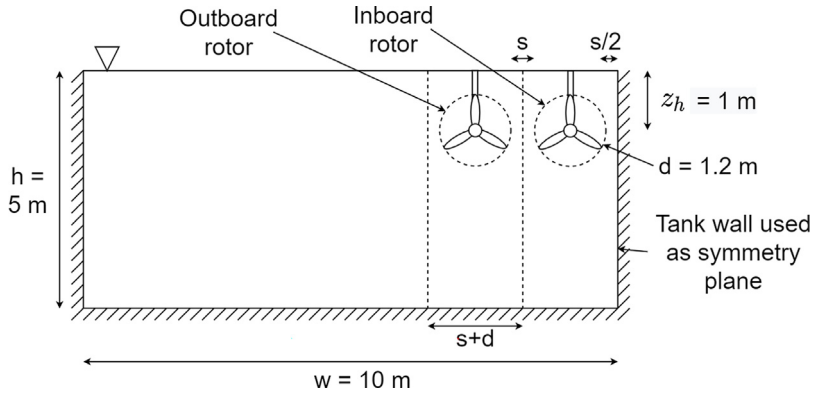

Fig. 2. Diagram of the turbine configurations in the towing tank at SSPA chosen to mimic a 4-turbine fence.

Fig. 2 describes the setup of the turbines for this study. The turbines were mounted on a steel beam held underneath the tow carriage, along which the turbines could be slid to adjust their cross-stream positions, as shown in Fig. 3. By changing the lateral positions of the turbines we were able to investigate the effect of turbine spacing in fences. Three inter-turbine spacings s were considered, $s/d = 0.25, 0.72, 1$. For each inter-turbine spacing, the tip-to-wall distance was $s/2$, so that through symmetry a fence of four evenly spaced turbines was presented. The turbines were positioned with their rotational axes $z_h = 1$ m below the free surface, giving a minimum tip submersion depth of $z_t = 0.4m = d/3$, which was chosen to match the tip submersion depth in our previous experiments at FloWave (McNaughton et al., 2019).

2.3. Test conditions

All tests were performed at steady carriage speeds of 0.8, 0.9 and 1.0 m/s. Tests were performed in the TSR range 5.5 to 8.2, with rotational speeds between 70 and 106.25 rpm depending on the carriage tow speed. A five-hole probe, supplied by SSPA, was used to determine flow conditions upstream of the rotors. Turbulence intensities ranged between 0.25 and 1.65% with the majority in the range 0.6–1.2%. Several test points were repeated over the course of the experimental campaign to understand repeatability of the data while also considering the effect of the wait time between each tow. Some data variability was observed between tows although it was not possible to determine any direct correlation with wait time due to the slow build up of unsteadiness over multiple tows, which is expected to vary with turbine operation, i.e. thrust. Whereas the maximum turbulence intensity fell with increasing wait time between tows, the minimum values were observed at the lowest and highest wait times. Furthermore, there were (non operational) wave makers at the end of the tank which would reflect any bow wave produced by the turbines back towards them. For the purpose of this study, only data points with a wait time between 10 and 30 min are included, with any repeated data points averaged at a given TSR.

3. Analysis

3.1. Data acquisition and processing

The rotor and blade load signals were routed through a noisy environment susceptible to electromagnetic interference (EMI) due to passing through the slip ring and alongside the motor cables before reaching the data acquisition system over approximately 10 m of cable. To reduce signal attenuation, and also reduce the number of cable strands, amplifiers fitted close to the strain gauges were used to convert voltage differentials to a current output (4–20 mA). These regulated the excitation voltage for the strain gauge bridges and removed sensitivity to EMI and the potential for voltage drop over the cable length.

Prior to each test run, a 20 s file was recorded to provide a zero for each sensor. To avoid amplification of noise, a standardised technique was adopted of processing each sensor's output prior to zeroing and multiplying by calibration factors. Two digital filters were adopted, a Hampel filter to remove outliers and a low pass filter to remove frequencies greater than 12 times the rotational frequency. Owing to noisy data the Hampel filter was applied both before and after the low pass filter.

In part due to the limited space inside the turbine nose, the RBM transducers were machined to have relatively thin flanges and the strain gauges were positioned close to the mounting holes. This resulted in some sensitivity of the transducers to the mounting bolt torques when installed, which affected the calibration slopes of the RBM transducers after turbine assembly when compared to those obtained in laboratory bench tests. To address this issue, a post-test calibration technique was applied to the RBM data that scaled the flapwise moments using the whole rotor thrust, and

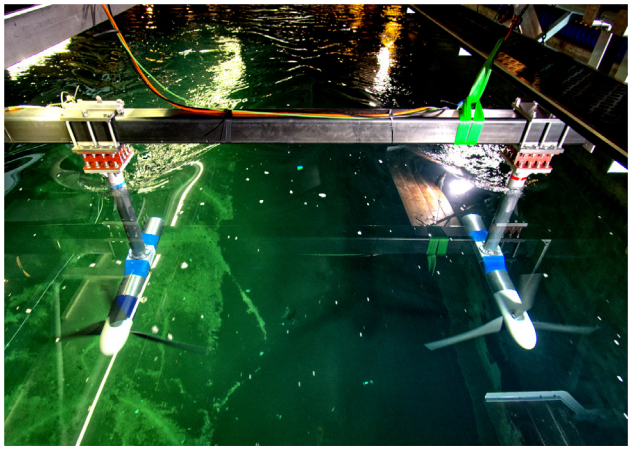

Fig. 3. Photograph of the turbines operating at inter-turbine spacing $s/d = 1$. The right hand turbine is the inboard rotor.

the edgewise moments using the whole rotor torque. To apply the technique, the mean RBM data for each tow was plotted against the mean rotor thrust or torque. For each blade and load direction, a scale factor was calculated as the ratio between the ideal RBM-load slope and the measured slope, and the RBM adjusted accordingly. The ideal slopes for the flapwise and edgewise moments respectively are $(T/3)r_T$ and $Q/3$, with T the rotor thrust, Q the rotor torque and r_T is the radial point of action of the thrust force on the blade. A value of $r_T = d/3 = 0.4$ m was determined from the blade-load distributions obtained from the CFD used in rotor design. The ideal slope assumes that all three blades make an equal contribution to the rotor load. Whilst this may not be true at any given instant, due for instance to blade passing and surface proximity effects, it only introduces small error when considering the time mean load experienced over an entire test run of more than 100 shaft rotations. Additionally, the approach assumes no geometric or mounting differences between blades, which could arise due to manufacturing tolerances.

3.2. Performance metrics

For the purpose of interpreting the results, the TSR, thrust and power coefficients are defined as:

$$\lambda = \frac{\omega R}{U}, \quad C_T = \frac{T}{1/2\rho U^2 A}, \quad C_P = \frac{Q\omega}{1/2\rho U^3 A} \tag{1}$$

with ω the rotational speed [rad/s], T the rotor thrust [N], Q the rotor torque [Nm], R the blade radius [m], ρ the water density [kg/m^3] and A the turbine's swept area [m^2]. For the purpose of this study, the reference velocity, U [m/s] is taken as the programmed carriage speed. Time averages of rotor speed, thrust and torque were used to calculate the performance metrics. After removing transient effects due to acceleration and deceleration phases of the carriage and turbines, there remained between 120 and 180 s of usable data from each tow for time averaging; this varied according to carriage speed, turbine rotational speed and carriage start and stop positions. The above coefficients are generally defined as turbine specific, although it is also relevant to speak in terms of overall fence performance, which is taken as the average of the respective coefficients for both the inboard (near tank side wall) and outboard (closer to tank centre) rotors as defined in Fig. 2. Finally, to assess the overall efficiency of the fence, the basin efficiency is defined as:

$$\eta = \frac{C_{P,F}}{C_{T,F}} \tag{2}$$

with $C_{T,F}$ and $C_{P,F}$ the fence-averaged thrust and power coefficients respectively. The basin efficiency represents the ratio of the power usefully generated from the flow to the total power removed from the flow which necessarily includes viscous loses and the power lost in wake remixing.

We present blade loads as phase averages across all 3 blades of the rotor. The time series of each RBM signal is split according to shaft position into one-degree bins with the data in each bin averaged. The self-weight of the blade is calculated using the CAD file outputs for mass and volume and the contribution this makes to the edgewise RBM at each azimuthal position subtracted from this component's phase average. The three blades are combined by correcting the phase so zero degrees is vertically upwards for all three blades and then averaged.

3.3. Experimental uncertainty

We consider that the majority of experimental uncertainty arises from the towing data (test uncertainty), i.e. in relation to unsteady flow effects from the test setup and from noise and vibrations during the towing. The effect of the model assembly, sensors and test set up is considered small in comparison to these. Further detail is given in Appendix B.

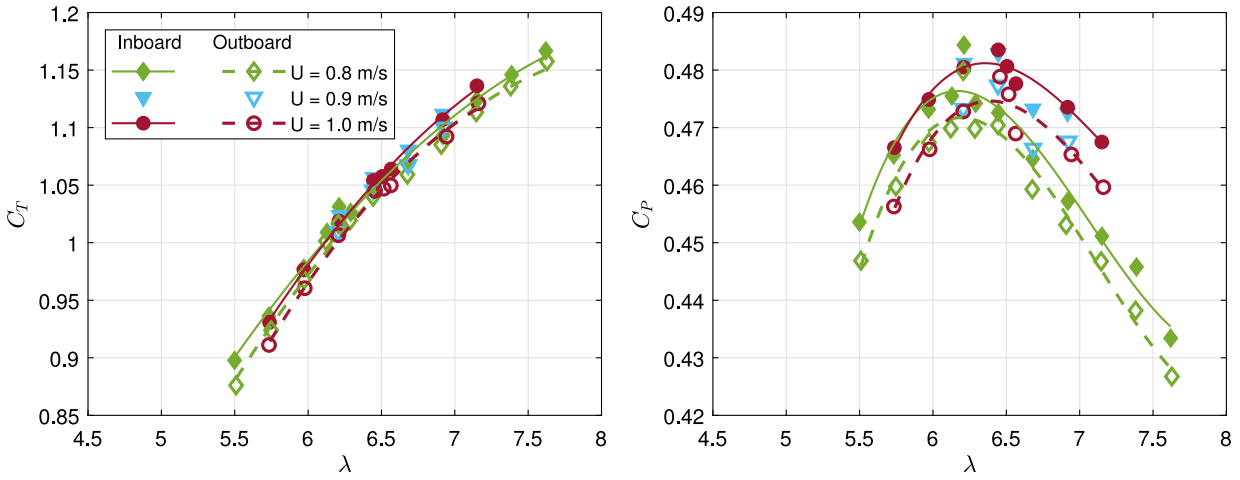

(a) Thrust coefficient. (b) Power coefficient.

Fig. 4. (a) Thrust and (b) power coefficients as a function of tip-speed ratio for different tow speeds with $s/d = 0.25$. Lines indicate second- and third- order polynomial fits to the thrust and power coefficient data respectively.

There is generally good repeatability of the tests, although we observe a generally higher variation for the inboard turbine, higher variability for the larger spacing, and higher variability for the power coefficient. The standard deviation of performance coefficients over repeated tests is generally less than 1% of the mean, although the inboard turbine shows higher variation at the larger spacing. The standard deviations of the time series data do not show dependence on TSR nor inter-turbine spacing, and as a percentage of the mean are in the range 0.8–2.4% for TSR, 1.0–2.0% for thrust coefficient, and 2.5–6.1% for the power coefficient.

3.4. Reynolds number dependency

Previous tests with this rotor (McNaughton et al., 2019) demonstrated Reynolds number independent performance at flow speeds of 0.7 m/s and above. However, those tests were conducted in the FloWave flume which has relatively high levels of turbulence which are not expected in a towing tank. The majority of tests conducted in the current experiments were at 0.8 m/s in order to retain consistency with the design (Cao et al., 2018) and previous tests (McNaughton et al., 2019) as well as respecting the design limits of the sensors. A brief investigation into the effect of tow speed on results was conducted for a limited TSR range at $s/d = 0.25$. Thrust and power coefficients are presented for a range of tow speeds in Fig. 4 for both the inboard and outboard rotors. Due to a reasonable amount of scatter in the data points, we fit second- and third- order polynomials to the data for the thrust and power coefficients, respectively. This exponent choice is to maintain the expected relationship between TSR and each of the coefficients. Curve fits are only applied to the 0.8 m/s and 1.0 m/s tow tests, at 0.9 m/s there are insufficient data points over the TSR range to define this polynomial.

The thrust coefficient shows little sensitivity to the tow speed and while separate curves are shown, a universal fit could apply to the union of all data. Comparing this universal fit to the separate curve fits demonstrated the curves are similar within a 5% significance level under a two-sample Kolmogorov–Smirnov test. Up to a TSR of approximately 6.2 the power coefficients remain relatively unscattered regardless of tow speed. However, at $\lambda = 6.2$ there is some scatter in the 0.8 m/s data. It is thought that at this TSR there are some transitional effects as a result of local variations in turbulence intensity and flow speed experienced. At this TSR the chord-based Reynolds number at 70% span is approximately 155,000 while the transitional Reynolds number for the selected profile is in the range of 100,000–200,000 and thus transitional effects in this low turbulence intensity environment may have been encountered as the turbines' TSR and hence blade Reynolds number were increased. For $\lambda > 6$ a clear difference in power coefficients is observed between at 0.8 m/s and 1.0 m/s. Although there is only a small amount of data available at 0.9 m/s, these data points are sufficiently close to the 1.0 m/s data points to indicate that there is Reynolds number independence at this tow speed.

The difference between inboard and outboard rotor performance is discussed in detail in Section 4.2. Here we draw attention to the fact that at all tow speeds there is a clear difference between the inboard and outboard rotors, with the inboard rotor producing higher values of thrust and power coefficients. While it appears that there is a Reynolds number effect in the results for $\lambda > 6.2$ for the 0.8 m/s tests, this is not believed to influence the overall conclusions of this work. In fact, owing to the difference between inboard and outboard rotor loads being observed to be greater at higher tow speeds, it is likely that the across-fence-effects discussed in latter parts of this paper will be more pronounced if fuller Reynolds number independence were achieved.

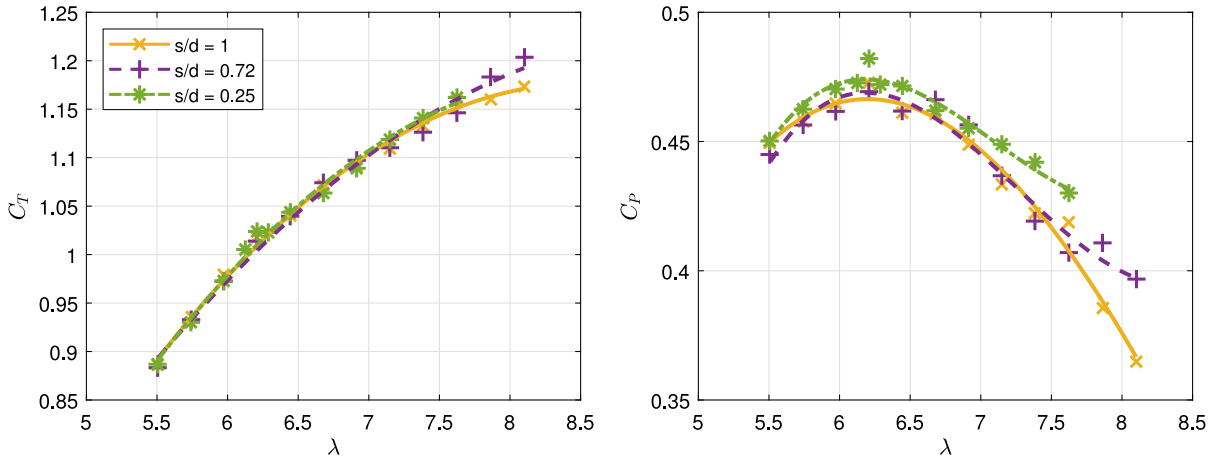

(a) Thrust coefficient. (b) Power coefficient.

Fig. 5. Fence-averaged performance for different inter-turbine spacings. (a) Thrust coefficient vs. tip-speed ratio, (b) power coefficient vs tip-speed ratio. Data are averaged across both turbines and lines indicate second- and third- order polynomial fits to the thrust and power coefficient data respectively.

4. Results

4.1. Fence performance

The fence-averaged performance coefficients for three inter-turbine spacings are shown in Fig. 5 as a function of TSR. At lower TSRs, there is little difference between the fence-averaged thrust coefficients. Although we only performed tests at $\lambda > 7.5$ for the two larger spacings, in this region the fence thrust coefficient exhibits a mild increase with decreasing spacing. The same trend is observed for the power coefficients, with the two larger spacings showing similar performance at lower and moderate TSRs, and increased performance with decreasing spacing at higher TSRs. The fence-averaged power coefficient for the closest spacing is consistently higher over the measured TSR range. Such increase in power with increasing local blockage (decreased spacing) agrees qualitatively with partial fence theory developed for infinitely long arrays of homogeneously operating turbines partially spanning a much wider channel (Nishino and Willden, 2012). As spacing is reduced, the expansion of each turbine-flow streamtube becomes more constrained, which increases the mass flux through each turbine. Increased turbine mass flux enables each turbine to support increased thrust, which it achieves by operating at higher TSR. The balance of increased thrust enabled by higher flow rate yields an increase in individual and fence-averaged power coefficient, as is observed in our experimental results presented in Fig. 5. For the results presented here, decreasing the spacing from $s/d = 1$ to 0.25 increases the maximum C_P by 1.4%, with the corresponding C_T increasing by 1.5%, which is achieved by increasing the TSR for peak power by 1.6%. While modest, this is a clear and sustained observation over the entire TSR range presented.

4.2. Effect of inter-turbine spacing

We next consider how turbine loading varies across the rotor fence. Returning to Fig. 4 we observe for the spacing, $s/d = 0.25$, that the inboard turbine loading and power are higher than those seen by the outboard turbine (by 0.9% and 1.0% for thrust and power respectively at peak performance, for a flow speed of 0.8 m/s). This is as we might expect and agrees qualitatively with previous numerical simulations (Vogel and Willden, 2017). We expect the inboard turbines to experience flow constraint effects from the turbines to either side of them, with those flow constraints leading to reduced streamtube expansion, higher mass flux, and in turn higher inboard turbine loads and power. The outboard turbines are only constrained on one side and hence experience less streamtube constraint, lower mass flux and thus lower power and thrust, than the inboard turbines. The overall fence performance might thus be characterised as a fence of constant thrust with superimposed fence end-losses reducing the performance of the outer most turbines due to around-fence flow leakage.

Whilst this appears to be true for the closest spacing, careful examination of the thrust and power coefficient demonstrates this is not the case for the other spacings tested. Fig. 6 shows that at the highest spacings it is the outboard turbine that experiences the highest loads and power, and that as the turbine spacing is reduced the inboard turbine increases in load and power until it exceeds that of the outboard turbine, but in the present study this is only achieved at the very closest spacing of $s/d = 0.25$. This is further highlighted through Fig. 7 which presents individual turbine as

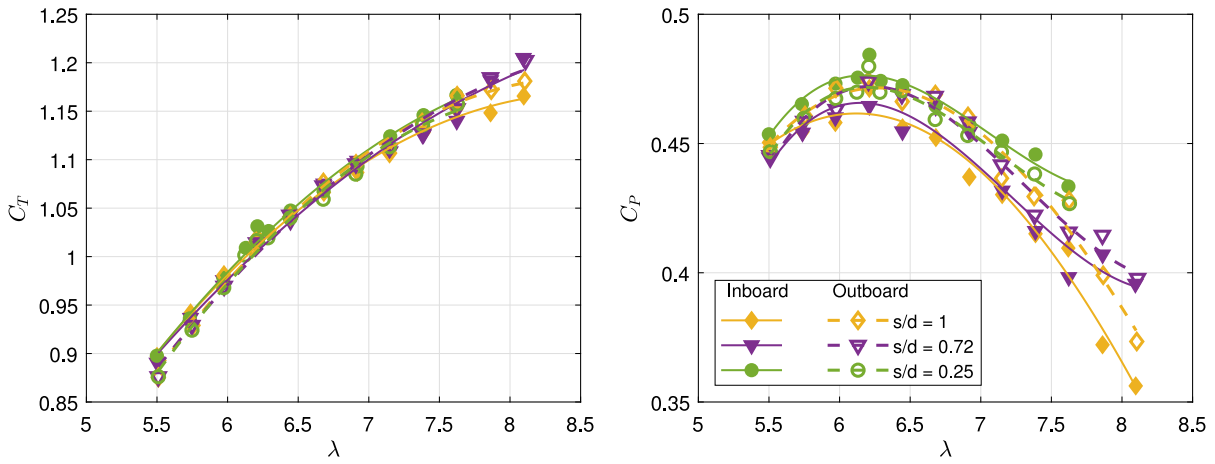

(a) Thrust coefficient. (b) Power coefficient.

Fig. 6. (a) Inboard and (b) outboard turbine performance for different inter-turbine spacings. Lines indicate second- and third- order polynomial fits to the respective thrust and power coefficient data for each turbine and spacing pair.

well as fence maximum power coefficients, together with the corresponding thrusts at which these are achieved, as a function of inter-turbine spacing.

This departure from the theoretical ideas around turbine fence end-losses postulated above, and computational observations of across-fence turbine thrust and power variations (Nishino and Willden, 2013; Vogel and Willden, 2017) is unexpected and may result from several effects. Clearly there is an assumption that the tank side wall provides a perfect symmetry plane. Whilst this is a well established technique in model testing, the boundary layer that inevitably develops between the tank side wall and the fluid upstream of the turbines, which is pushed forward ahead of the turbines in the inertial frame, may act to impede the flow through the inboard turbine relative to the outboard turbine, thus reducing loads and power across the middle of the pseudo four turbine array.

Also, the theoretical ideas around array performance are built on a two-scale representation of the flow problem in which the array-scale flow approaches uniformly across the width of the array, with subsequent across-array variation due to less constrained streamtubes of the outermost turbines. The assumption of uniformity of the approaching array flow may also be inaccurate, and simulations (Vogel and Willden, 2017) have demonstrated that the approaching array flow is non-uniform and decelerated at its centre, with relatively higher speed flows accelerating past the ends of the array. Again this would lead to relatively higher thrust and power of the outboard turbines due to increased flow speeds. We note though that if this were the sole reason for the increased performance of the outboard turbines at wider spacings, this would be inconsistent with computational observations of across-array performance (Vogel and Willden, 2017).

It is also acknowledged that slight differences in the manufacture, setup and installation of the two turbines may have occurred which could have given rise to small differences in performance between them.

However, it is clear that as the inter-turbine spacing is decreased, the performance of the inboard turbine is significantly elevated relative to its performance at wider spacings, and this we attribute to the greater constraint imposed on the inboard turbine's streamtube as its neighbouring turbines are brought closer towards it. Relative to the widest spacing, the inboard rotor at closest spacing experiences a 2.8% increase in power coefficient, which is achieved through a 1.8% increase in thrust and 2.9% increase in operating TSR. Conversely, the outboard turbine's performance remains relatively unaffected by changes to the inter-turbine spacing.

The fence's basin efficiency, which we recall is the ratio of power-to-thrust coefficients (Eq. (2)), is plotted as a function of fence power coefficient in Fig. 8(a). At the very lowest TSRs the basin efficiency is highest, and it gradually decreases with increasing TSR. It is clearly desirable to operate close to maximum power coefficient and here we note that all fence configurations achieve $\eta \approx 0.46$ at maximum power; see Fig. 8(b). We observe, that by decreasing the inter-turbine spacing it is possible to achieve a higher power coefficient for any given basin efficiency. This is beneficial to the overall system as loads and impact on the resource can be maintained whilst increasing the power that can be usefully generated. This could be readily explored by the tidal energy industry to improve performance. Comparing the basin efficiency at maximum power coefficient (Fig. 8(b)) for the different spacings, we observe that while the fence-averaged value is relatively independent of spacing, the difference between the individual rotor's basin efficiency decreases with spacing. Hence, for the rotor system presented here, the closer spacing of $s/d = 0.25$ provides the most even across-fence ratio of power-to-thrust.

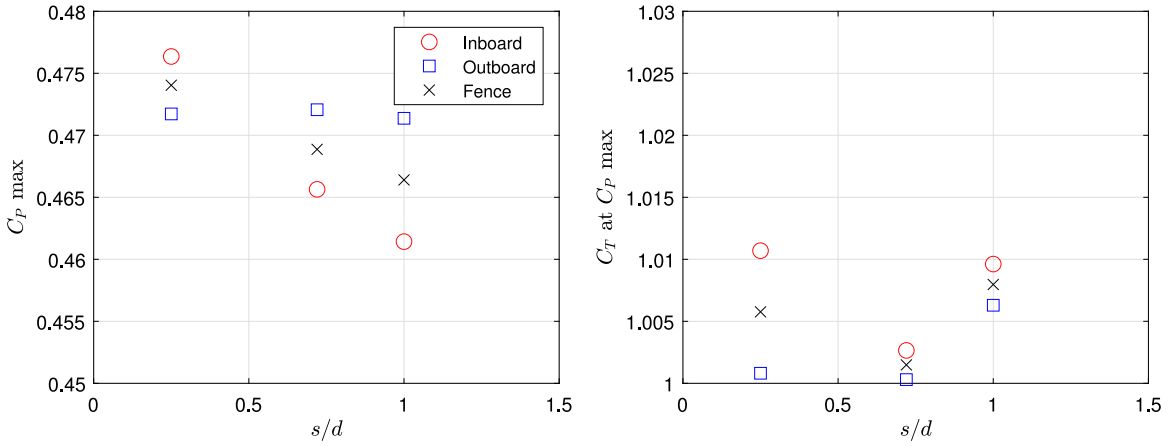

(a) Maximum power coefficient dependency on inter-turbine spacing.

(b) Thrust coefficient at maximum power coefficient as a function of inter-turbine spacing.

Fig. 7. (a) Maximum power coefficient for each fence spacing and (b) associated thrust coefficient.

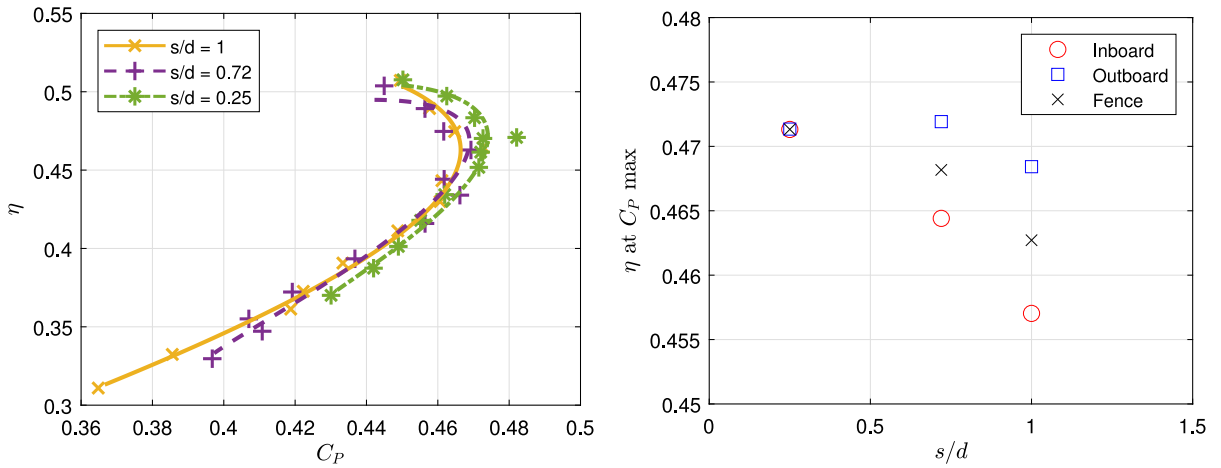

Fig. 8. Demonstration of array efficiency through (a) basin efficiency for each fence spacing and (b) associated value at maximum power coefficient.

4.3. Blade loading

Figs. 9 and 10 show the azimuthal variation in flapwise and edgewise RBM respectively for the inboard and outboard turbines at different spacings and for three TSRs that represent a range of points over the performance curves, $\lambda = 5.50$, 6.44 and 7.15. The RBM values are normalised by the fence-averaged azimuthal-mean values at $s/d = 1$ in order to highlight the differences between the turbines and the changes that arise as inter-turbine spacing is varied.

The rotors experience interference effects due to their proximity to one another and the tank side wall, which can be seen in localised peaks in the flapwise and edgewise RBMs. For the outboard rotor, decreasing the inter-turbine spacing leads to an increase in RBM loads on the side towards the inboard turbine; for flapwise load this occurs between 225° and 270°, and for edgewise around and just after 270°. The angular location of the edgewise peaks thus lags that of the flapwise peaks. This pattern is also observed for the inboard rotor, where flapwise peaks occur a little ahead of the 90° and 270° locations, with edgewise interactions occurring a little later at closer to the 90° and 270° positions.

The magnitude of these interactional peaks increases as TSR, and thus overall thrust, is increased and also as the inter-turbine spacing between the rotors is reduced. Additionally, for both rotors, the location of these flapwise and edgewise peaks occur at later azimuthal positions with increasing TSR and thus turbine loads, so that peak loads occur when the rotor blades are closer to the horizontal, and thus the neighbouring rotor. Thus as the turbines exert greater resistance on the flow, the peak constructive interference effects between neighbouring turbines (and in our case the symmetry plane) become more significant, as indicated by the increase in magnitude peaks and their locations closer to the horizontal.

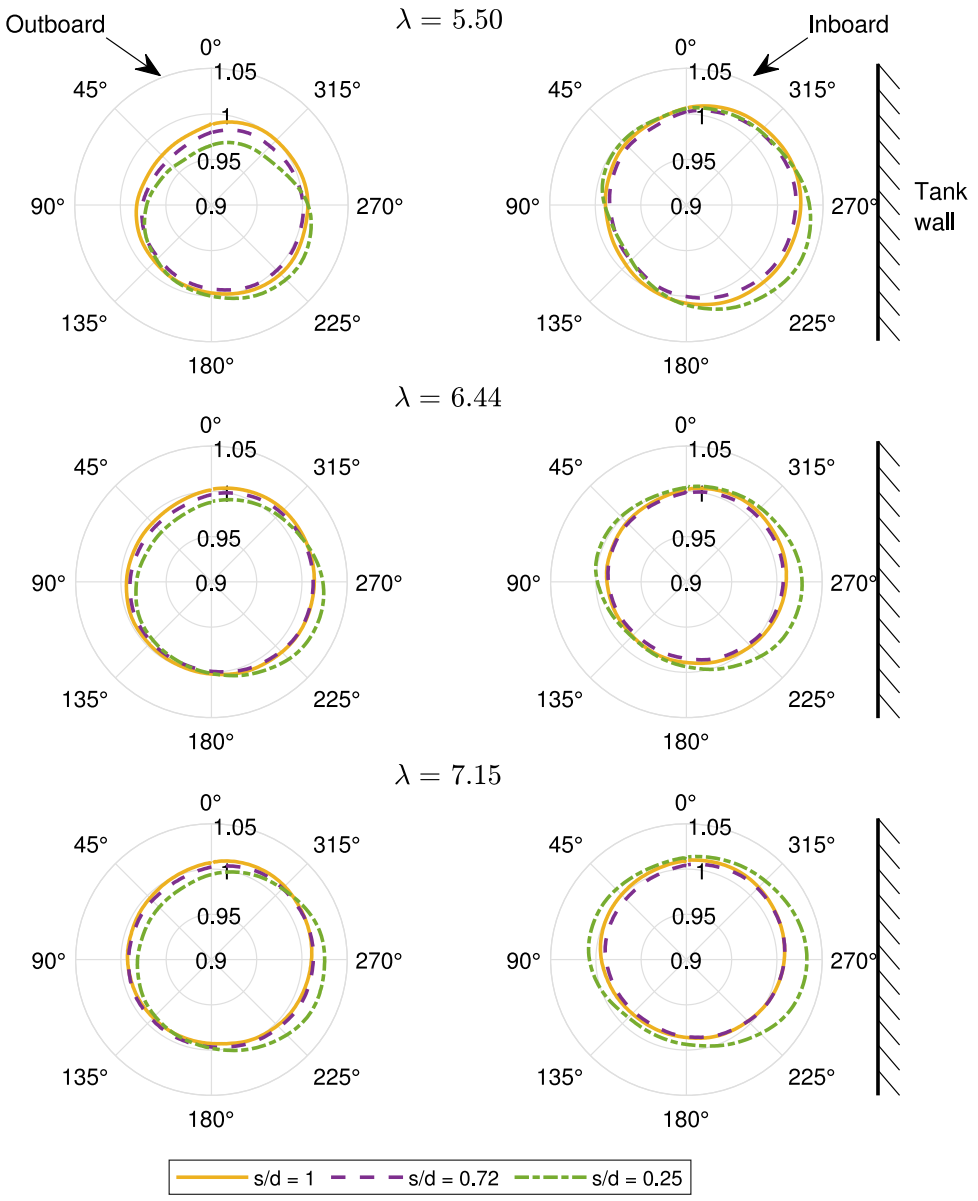

Fig. 9. Phase averaged flapwise root bending moments. Left hand plots are outboard turbine and right hand plots are inboard turbines. Each turbine's data is the average of the three individual blades, phase-averaged in 1° bins, and normalised by the fence-averaged azimuthal-mean at $s/d = 1$.

The interference effects are most obvious for the closest spacing of $s/d = 0.25$ for which turbine interactions result in horizontally ovalised flapwise and edgewise RBM patterns for the inboard rotor and laterally asymmetric RBM loading for the outboard rotor. The lateral asymmetry of the outboard rotor's loads helps explain, in part, the insensitivity of the outboard rotor's performance coefficients to changing the turbine spacing, suggesting that while the inboard side of the rotor experiences increased loading, there is a release on the outer side, potentially from bypass flow diverting around and underneath the rotors. While the constructive interference effect that the outboard rotor experiences is in the form of a single peak directed towards the inboard rotor, the inboard rotor experiences two peaks, one from the outboard rotor and the other from the tank side wall, in addition to an overall increase in loading around the full azimuth. It is this overall increase in load that allows the inboard rotor to exert a greater resistance to its approach flow to the overall benefit of turbine performance.

Fig. 11 shows a fast Fourier transform (FFT) of the flapwise root bending moment for each rotor at different spacing for $\lambda = 6.44$. The characteristic frequency (taken as the rotational frequency, f_0) is evident with higher harmonics up to $4f_0$ present for both rotors. Observations of these higher harmonics are expected for the blade RBMs (Payne et al., 2018). The

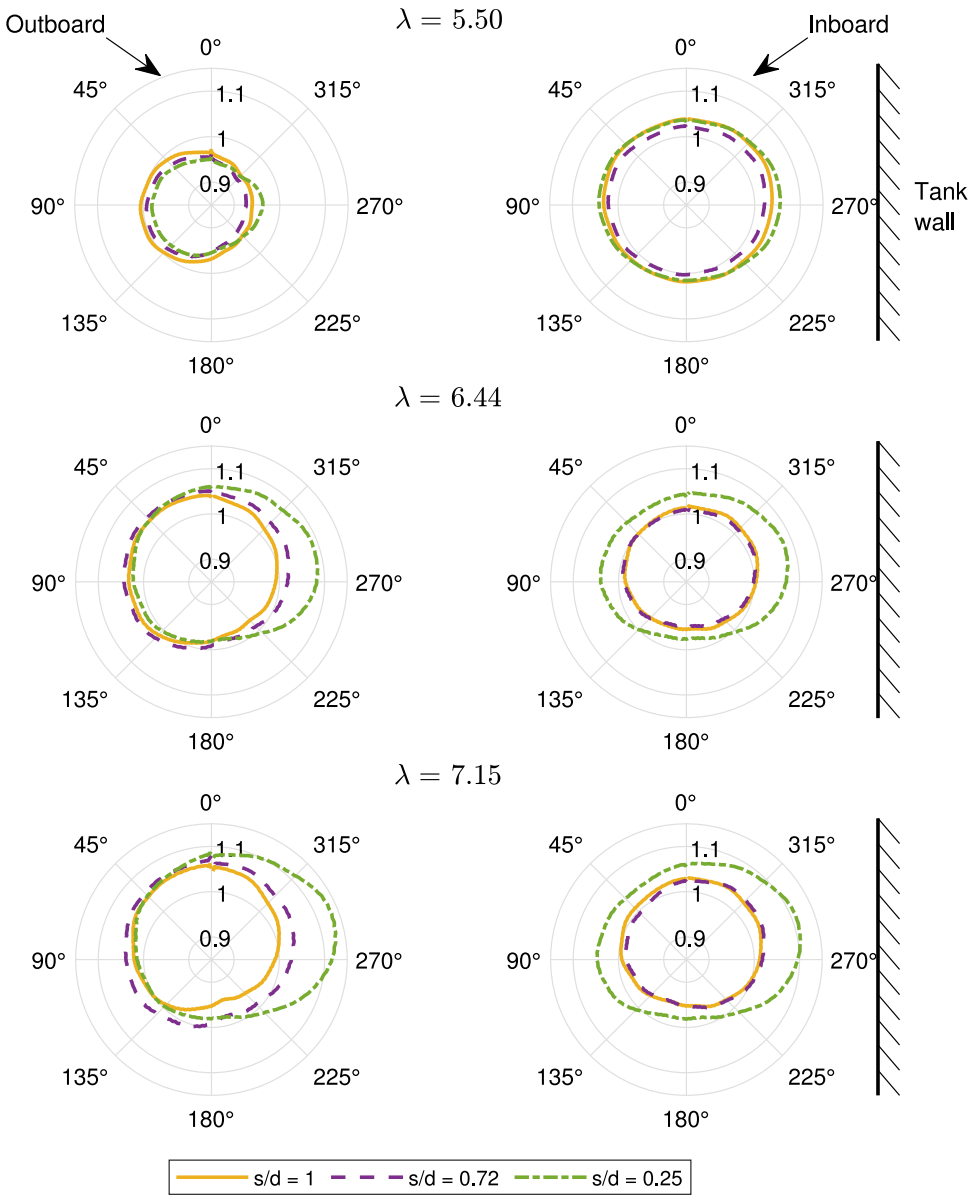

Fig. 10. Phase averaged edgewise root bending moments. Left hand plots are outboard turbine and right hand plots are inboard turbines. Each turbine's data is the average of the three individual blades, phase-averaged in 1° bins, and normalised by the fence-averaged azimuthal-mean at $s/d = 1$.

relative amplitudes of the harmonics are generally greater on the inboard rotor, with the exception of the third harmonic which is greater for the outboard rotor.

The normalised peak amplitudes of the first four harmonics are shown for the flapwise and edgewise loads for $\lambda = 6.44$ in Fig. 12 to demonstrate the effect of spacing on the loading harmonics of each turbine. Whilst the peaks at each harmonic are larger for flapwise, due to the higher out of plane bending, the load components, when normalised on the signal mean, are of a similar order of magnitude in both directions. This demonstrates that turbine-induced cyclic loading events have a similar effect in both loading directions.

In all but one instance, the amplitude of each harmonic increases with decreasing inter-turbine spacing as might be expected as the rotor-on-rotor interactions increase. The outlying data are for the outboard edgewise RBM at f_0, which decreases between the moderate to closest inter-turbine spacing. The cause of this is unclear from the available data, but may be one or more once-per-revolution load signals that act in different directions and thus combine to produce a lower overall magnitude. The blade self-weight (at its maximum at an azimuth of 90°), surface and tower passing effects (at and after approximately 0°) are potential contenders for these phenomena.

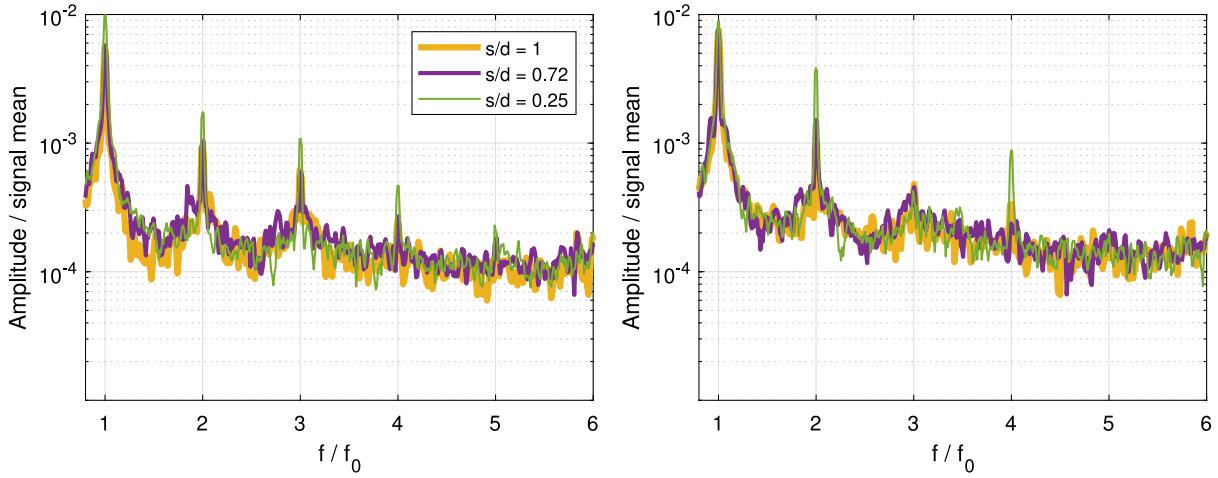

(a) Outboard rotor. (b) Inboard rotor.

Fig. 11. FFT for outboard (left) and inboard (right) flapwise RBM for a single blade at different spacings for $\lambda = 6.44$. Data is normalised by the mean blade's mean flapwise RBM at each spacing.

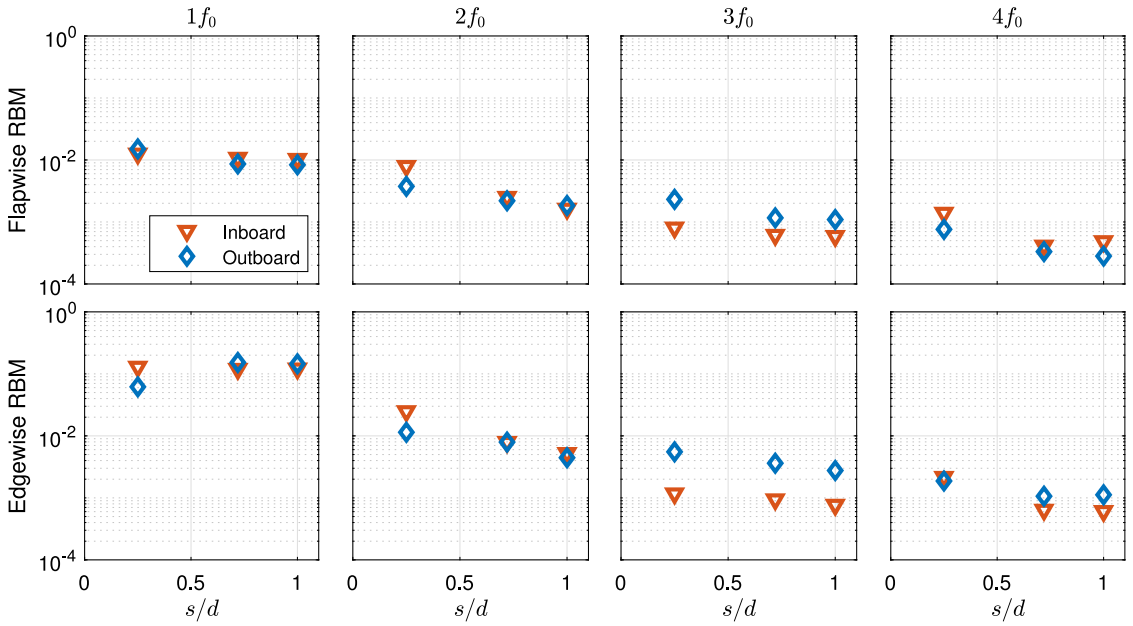

Fig. 12. Amplitude peaks from RBM FFTs at different harmonics of the characteristic frequency (f_0) as a function of turbine spacing (top = flapwise, bottom = edgewise). Data shown are for $\lambda = 6.44$ and averaged across all blades and normalised by the mean flapwise RBM at each spacing.

The greater rate of increase of the inboard rotor's even harmonics with decreased spacing is due to the inboard rotor experiencing enhanced interactions with rotors on both sides (here the outboard rotor and the tank wall), compared to the outboard rotor.

4.4. Differential control

The results presented in the preceding sections all used collective turbine control, whereby both turbines rotated at the same fixed rotational speed. However, it was observed that this resulted in the turbines experiencing different loads, fence-induced variations in the approach flow speed across the width of the fence. Such load variations may be undesirable in practice as it is likely that all turbines will be designed to the same loading conditions, resulting in over-engineered designs to meet the higher loads conditions, including peak and fatigue loading distributions. To understand how loads can be balanced across the fence, tests were performed at the $s/d = 0.25$ inter-turbine spacing using differential speed

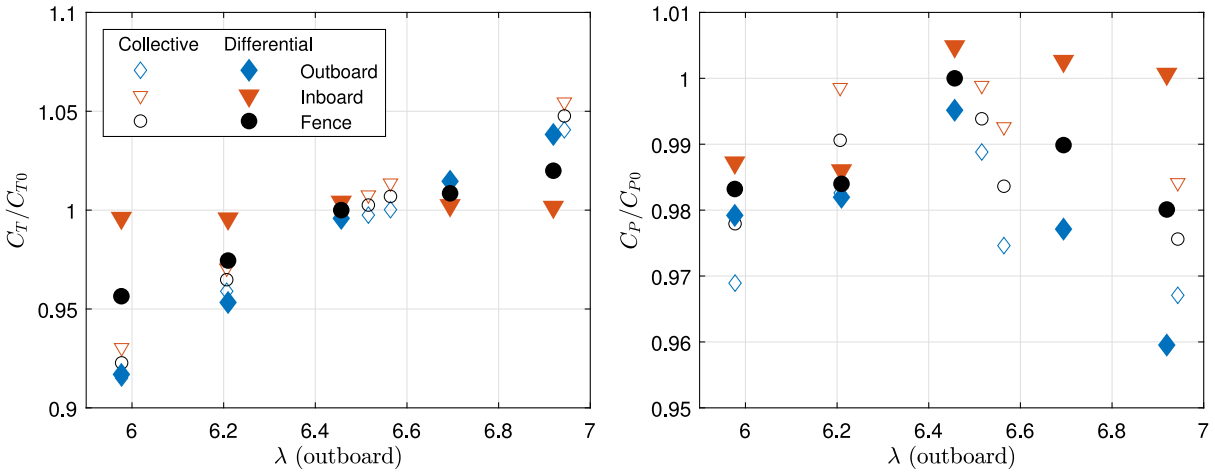

(a) Thrust coefficient. (b) Power coefficient.

Fig. 13. Variation in (a) thrust and (b) power coefficients as a function of outboard (variable) turbine's TSR for differential (thick lines) and collective (thin lines) control strategies. For differential control the outboard rotor's speed varies according to the x-axis, whilst the inboard rotor's speed remains constant at $\lambda = 6.44$. For collective control both rotors operate at the same speed indicated by the x-axis. Data are for a towing speed of 1.0 m/s and normalised by the corresponding thrust or power coefficients, C_{T0} and C_{P0}, for the collective controlled fence at $\lambda = 6.44$.

control, where the inboard rotor was kept at a constant rotational speed ($\lambda = 6.44$ based on the carriage tow speed) and the outboard rotor operated at speeds either side of this. Performance coefficients arising from these tests, and compared to the collective control results, are provided in Fig. 13 as a function of the outboard (variable) turbine's TSR. Note that these results are all for a towing speed of 1.0 m/s.

The thrust coefficient of the outboard rotor appears insensitive to whether the inboard rotor is operated at a fixed $\lambda = 6.44$ (differential control) or at the same TSR as the outboard turbine (collective control). For differential control, and therefore constant inboard rotor TSR, there is some minor variation in the inboard rotor's thrust loading, although these variations are likely to lie within experimental uncertainty. The outboard rotor power coefficient curves are again quite similar regardless of the control strategy, although the shape of the curve and the dissimilar measurement points do give the impression of more erratic behaviour. The inboard rotor power coefficient does exhibit an interference effect by varying the load (and TSR) of the outboard rotor. However, within the discrete range of rotor speeds tested, no combination of differential control leads to a net increase in the overall power delivered by the fence relative to the peak fence performance with collective control. This is contrary to expectations, as other works (Vogel and Willden, 2017) have shown that adjustments to thrust variation across a fence can achieve a net fence-power increase. However, such increases and adjustments are small and may be undetectable within the range of discrete sampling points and experimental error. In the present study, the resulting fence performance is thus maximised when both rotors are operated at the same TSR; a further investigation could examine how a variable inboard turbine effects the outboard loading.

5. Conclusion

Tests have been carried out on a four turbine array, achieved by towing two model turbines through a long still water towing tank, and using the tank's side wall as a symmetry plane to provide a pseudo four turbine array through reflective symmetry. To the authors' knowledge, this is the first study of its kind for tidal turbine investigations, although the use of symmetry planes is commonplace in numerical simulations.

By suspending the turbines from above and adjusting their cross-stream positions, the effect of inter-turbine spacing on the array was investigated. As is expected from theoretical analysis of fences partially spanning the width of wider channels, decreasing the inter-turbine spacing, which increases the local blockage, was observed to have a beneficial effect on overall fence performance. It was observed that decreasing the spacing from one diameter to a quarter of a diameter resulted in a modest but sustained increase in power coefficient over the full range of TSRs tested. The fence averaged power coefficient was observed to increase by 1.4%, which was achieved largely through a 2.8% increase in the inboard turbine's power coefficient. As the inter-turbine spacing was reduced the operating TSR and thrust coefficient for peak fence power increased by 1.6% and 1.5% respectively, demonstrating the capacity of the turbines to support and exploit higher loads when the turbine flow expansions are constrained by close side-by-side operation.

In the closest spacing it was observed that the inboard turbine exhibited a higher thrust load, and power, than the outboard turbine, which agrees with prior simulation results of turbine fences and is consistent with the idea that the inner turbines are constrained on both sides, whilst the outboard turbines experience some load relief on their open

side. However, at wider inter-turbine spacings this was not the case and the outboard turbine experienced higher thrust and power. The reasons for this are unknown but the imperfect symmetry plane and experimental set up inaccuracies may have contributed to departures from expectations. However, the inability to make sufficient flow measurements in a towing tank of this scale render us unable to fully quantify or investigate these deficiencies further. Nevertheless, as we considered the incremental change between turbine spacings, our overall conclusions remain unaffected. Further investigation of the use of the side wall as a symmetry plane for turbine fence experiments is desirable as a future research topic.

Edgewise and flapwise root bending moment sensors were used to record the azimuthal variation in blade root bending moments. Analysis reveals peak blade loading when each blade passed in proximity to the neighbouring turbine and tank side wall. Thus the inboard turbine experienced twice as many loading peaks as the outboard turbine. The magnitude of the peaks increased with decreased inter-turbine spacing and increased TSR, both of which acted to increase mean load. Additionally, the azimuthal positions of loading peaks rotated to closer to horizontal as the TSR was increased or spacing reduced, indicating that they were driven by interference with the neighbouring turbine which is passed closest to at the horizontal.

The effect of differential testing demonstrated that the outboard rotor can affect loading on the inboard turbine, although the overall influence was small. Ultimately, as shown in McNaughton et al. (2019) there is potential to balance power production within an array of turbines by using differential speed control. However, the limited TSR range conducted here for the differential control tests, and conducted only with the inboard rotor at a single TSR, means that whilst the present work is able to demonstrate the existence of a load-balancing effect through differential control, further work is required to quantify the extent to which balancing can be affected.

Reynolds number independence was examined by testing at different tow speeds. While a towing speed of 0.8 m/s appears appropriate for TSRs below 6.2, discrepancies in data at this TSR suggest transitional effects. Performance data at 0.9 m/s appear to be more independent of tow speed suggesting Reynolds number independence was only achieved at higher TSRs at and above this flow speed. However, we do not believe that this affects the principal conclusions of this work as similar observations on the effects of inter-turbine spacing were made at all flow speeds.

This paper expands on the twin turbine experiments presented in McNaughton et al. (2022) by expanding from two to four turbines. The same rotors were used but the present experiments were performed in a different facility with approximately half the global blockage (4.5%), a reduction in local blockage from 37.7% to 15.1% at the same quarter diameter inter-turbine spacing, and a much lower diameter-to-tank-depth ratio. Additionally, the present tests were performed in a towing tank rather than flume, and so turbines experienced significantly lower levels of ambient turbulence. For this reason, a direct comparison of turbine performance cannot be made, although we do note that the maximum and minimum power coefficients observed in these tests are bounded by the single and twin turbine data presented in McNaughton et al. (2022). Furthermore, as observed by Gaurier et al. (2020), it is expected that a flume with higher ambient turbulence levels will present higher performance coefficients than similar tests in a towing tank by promoting earlier transition to turbulence in the blade boundary layers. In addition to the four turbine tests presented in this paper, we conducted tests in the centre of the tank of the two turbine array, and future work will compare results from these tests directly with results from our FloWave tests.

This work extends the understanding of array performance from disc-based modelling such as Nishino and Willden (2012) to demonstrate the importance of blade-passing interactions when exploiting local blockage effects with real turbines. Our work also demonstrates the differences in performance between inboard and outboard turbines due to fence end effects which are also important to consider when developing turbine arrays.

CRediT authorship contribution statement

J. McNaughton: Data curation, Funding acquisition, Investigation, Methodology, Software, Formal analysis, Visualisation, Writing – original draft, review & editing. **S. Ettema:** Investigation, Formal analysis, Visualisation, Writing – review & editing. **F. Zilic de Arcos:** Investigation, Writing – review & editing. **C.R. Vogel:** Conceptualization, Funding acquisition, Investigation, Methodology, Writing – review & editing. **R.H.J. Willden:** Conceptualization, Funding acquisition, Investigation, Methodology, Writing – review & editing, Supervision.

Declaration of competing interest

The authors declare that they have no known competing financial interests or personal relationships that could have appeared to influence the work reported in this paper.

Data availability

Data will be made available on request.

Acknowledgments

RHJW would like to acknowledge UK EPSRC grant no. EP/R007322/1 who support his fellowship and funded this work. Facility access was funded by the H2020 MaRINET2 Transnational Access Program project number 3007.

Table 1
List of components used for the turbine models. Asterisk indicates some customisation for component with part no. closest off the shelf equivalent.

Component	Manufacturer	Part no.	Information
Motor	Moog	G-3-M6	
Servo drive	Moog	G392-004A	
Gearbox	Wittenstein	NP-025 MF2–20	Supplied by Moog with motor
Thrust & torque transducer (TTD)	Applied Measurements	DBBSS/TSF*	Custom load range & connectors
Shaft encoder	Industrial Encoders Direct	90-HA*	Custom cable exit to fit nacelle
Slipring	Servotecnica	SVTS C 04 00/24	
Shaft coupling	Mayr	Smartflex 2/932.433	
Data acquisition	National Instruments	Various	Used to control servo drive and log sensor data

Appendix A. Turbine components

For the purpose of supporting further researchers, a list of the key components used to construct the turbine models are listed in Table 1.

Appendix B. Experimental uncertainty

B.1. Sensor uncertainty

Thrust and power coefficients are based on measurements using the TTD and the encoder (power coefficient only). Additionally, both coefficients are calculated assuming a constant carriage towing speed, which is given as ± 1 mm/s by the facility, approximately 0.1% of the desired carriage speed.

Calibration of the TTDs was performed by the manufacturer, and exhibited almost-perfect linear behaviour for both loading directions and without hysteresis. This calibration included applying loads in 10% increments of the full load range between maximum and minimum for both thrust and torque. Cross talk on the transducer, i.e. the interference of a thrust load on the torque measurement and vice versa, was deemed negligible at 1×10^{-4} N m/N for torque and 6×10^{-2} N/N m for thrust, which corresponds approximately to 0.017 for C_T and 0.0065 for C_P.

A calibration check of the TTDs was performed in the laboratory after the test campaign. Loads were applied using 1 kg M1 class calibration weights (tolerance ± 50 mg) which were placed on the sensor for thrust loading, calibrating in compression only, and hung off a lever arm for torque. The gradient of the manufacturer-supplied calibration curve fitted the data from the laboratory check with an R^2 of unity to three decimal places.

The encoder had a resolution of 720 pulses per revolution and used quadrature decoding to give a resolution of 1/8°. For the highest shaft speed of 106.25 rpm and sampling frequency of 125 Hz the resolution was equivalent to 5.1°/sample and such the resolution was more than sufficient to give the required accuracy and resolution in measuring the angular speed and position of the shaft.

B.2. Model uncertainty

Precision was ensured in the model assembly through use of alignment pins for angles and lips for concentric components. A small L-plate was fixed to the tower top which ensured alignment of the turbine towers with the cross beam. It is thus considered that any misalignment in the turbine components and assembly of models in the tank was minimised within machine tolerance. Importantly, any misalignment would have thus been carried through all tests consistently ensuring a high precision of results from the model setup and making results comparable between the different inter-turbine spacings as desired.

B.3. Test uncertainty

Test uncertainty is considered for individual time series and the repeatability of tests. For each test run, the standard deviation of the non-dimensional quantities are calculated as:

$$\sigma_\lambda = \frac{\sigma_\omega R}{U}, \quad \sigma_{C_T} = \frac{\sigma T}{1/2\rho U^2 A}, \quad \sigma_{C_P} = \frac{Q\omega}{1/2\rho U^3 A}\sqrt{\left(\frac{\sigma_Q}{Q}\right)^2 + \left(\frac{\sigma_\omega}{\omega}\right)^2 + 2Q \star \omega \frac{\sigma_Q \sigma_\omega}{Q\omega}} \tag{3}$$

with σ_x indicating the standard deviation of variable x and $Q \star \omega$ the cross-correlation between Q and ω. The standard deviations do not show dependence on TSR or inter-turbine spacing and as a percentage of the mean are in the range 0.8–2.4% for TSR, 1.0–2.0% for thrust coefficient, and 2.5–6.1% for the power coefficients.

Repeatability is assessed only for tests which were performed multiple times under the same conditions, i.e. rotational speed, carriage speed, inter-turbine spacing and wait time. Three repeats were performed at each spacing for a rotational speed of 82 rpm, carriage speed of 0.8 m/s, wait time of 10–20 min. For each spacing, the standard deviation of the set of three performance coefficients, denoted by curly parenthesis, is shown as a percentage of their mean in Table 2.

Table 2
Variation in performance coefficients for repeated tests. The standard deviation of the set of repeated tests, denoted by curly parenthesis, is shown as a percentage of their mean.

Spacing	Inboard			Outboard		
s/d	$\sigma\{\lambda\}$	$\sigma\{C_T\}$	$\sigma\{C_P\}$	$\sigma\{\lambda\}$	$\sigma\{C_T\}$	$\sigma\{C_P\}$
1.00	0.0%	1.4%	3.8%	0.0%	0.1%	0.9%
0.72	0.0%	0.3%	0.8%	0.0%	0.2%	0.5%
0.25	0.0%	0.5%	0.8%	0.0%	0.4%	0.6%

References

Bahaj, A.S., Molland, A.F., Chaplin, J.R., Batten, W.M.J., 2007. Power and thrust measurements of marine current turbines under various hydrodynamic flow conditions in a cavitation tunnel and a towing tank. Renew. Energy 32 (3), 407–426. http://dx.doi.org/10.1016/j.renene.2006.01.012.

Cao, B., Willden, R.H.J., Vogel, C.R., 2018. Effects of blockage and freestream turbulence intensity on tidal rotor design and performance. In: 3rd International Conference on Renewable Energies Offshore. pp. 127–135.

Cooke, S.C., Willden, R.H.J., Byrne, B.W., Stallard, T., Olczak, A., 2015. Experimental investigation of thrust and power on a partial fence array of tidal turbines. In: Proceedings of the 11th European Wave and Tidal Energy Conference. Nantes, France.

Garrett, C., Cummins, P., 2007. The efficiency of a turbine in a tidal channel. J. Fluid Mech. 588, 243–251. http://dx.doi.org/10.1017/S0022112007007781.

Gaurier, B., Ordonez-Sanchez, S., Facq, J.-V., Germain, G., Johnstone, C., Martinez, R., Salvatore, F., Santic, I., Davey, T., Old, C., Sellar, B., 2020. MaRINET2 tidal energy round robin tests—performance comparison of a horizontal axis turbine subjected to combined wave and current conditions. J. Mar. Sci. Eng. 8 (6), 463. http://dx.doi.org/10.3390/jmse8060463.

Hunter, W., Nishino, T., Willden, R.H.J., 2015. Investigation of tidal turbine array tuning using 3D Reynolds-averaged Navier–Stokes Simulations. Int. J. Mar. Energy 10, 39–51. http://dx.doi.org/10.1016/j.ijome.2015.01.002.

Kolekar, N., Vinod, A., Banerjee, A., 2019. On blockage effects for a tidal turbine in free surface proximity. Energies 12 (17), 3325. http://dx.doi.org/10.3390/en12173325.

Li, Y., Calışal, S.M., 2010. Modeling of twin-turbine systems with vertical axis tidal current turbines: Part I—Power output. Ocean Eng. 37 (7), 627–637. http://dx.doi.org/10.1016/j.oceaneng.2010.01.006, URL: https://www.sciencedirect.com/science/article/pii/S0029801810000144.

McNaughton, J., Cao, B., Nambiar, A., Davey, T., Vogel, C.R., Willden, R.H., 2022. Constructive interference effects for tidal turbine arrays. J. Fluid Mech. 943, A38. http://dx.doi.org/10.1017/jfm.2022.454.

McNaughton, J., Cao, B., Vogel, C.R., Willden, R.H.J., 2019. Model scale testing of multi-rotor arrays designed to exploit constructive interference effects. In: Proceedings of the 13th European Wave and Tidal Energy Conference. Napoli, Italy.

Nishino, T., Willden, R.H.J., 2012. The efficiency of an array of tidal turbines partially blocking a wide channel. J. Fluid Mech. 708, 596–606. http://dx.doi.org/10.1017/jfm.2012.349.

Nishino, T., Willden, R.H.J., 2013. Two-scale dynamics of flow past a partial cross-stream array of tidal turbines. J. Fluid Mech. 730, 220–244. http://dx.doi.org/10.1017/jfm.2013.340.

Noble, D.R., Draycott, S., Nambiar, A., Sellar, B.G., Steynor, J., Kiprakis, A., 2020. Experimental assessment of flow, performance, and loads for tidal turbines in a closely-spaced array. Energies 13 (8), 1977. http://dx.doi.org/10.3390/en13081977.

Olczak, A., Stallard, T., Feng, T., Stansby, P., 2016. Comparison of a RANS blade element model for tidal turbine arrays with laboratory scale measurements of wake velocity and rotor thrust. J. Fluids Struct. 64, 87–106. http://dx.doi.org/10.1016/j.jfluidstructs.2016.04.001.

ORE Catapult, 2018. Tidal Stream & Wave Energy Cost Reduction & Industrial Benefit Report. Technical Report.

Payne, G.S., Stallard, T., Martinez, R., 2017. Design and manufacture of a bed supported tidal turbine model for blade and shaft load measurement in turbulent flow and waves. Renew. Energy 107, 312–326. http://dx.doi.org/10.1016/j.renene.2017.01.068.

Payne, G.S., Stallard, T., Martinez, R., Bruce, T., 2018. Variation of loads on a three-bladed horizontal axis tidal turbine with frequency and blade position. J. Fluids Struct. 83, 156–170. http://dx.doi.org/10.1016/j.jfluidstructs.2018.08.010.

Schluntz, J., Willden, R.H.J., 2015. The effect of blockage on tidal turbine rotor design and performance. Renew. Energy 81, 432–441. http://dx.doi.org/10.1016/j.renene.2015.02.050.

Vogel, C., Willden, R., 2017. Multi-rotor tidal stream turbine fence performance and operation. Int. J. Mar. Energy 19, 198–206. http://dx.doi.org/10.1016/j.ijome.2017.08.005.